

# New Approach for Target Locations in the Presence of Wall Ambiguities

GENYUAN WANG

MOENESS G. AMIN, Fellow, IEEE

YIMIN ZHANG, Senior Member, IEEE  
Villanova University

**A technique for target location estimation in through-the-wall radar imaging applications is presented. The algorithm corrects for the shifts in target positions due to ambiguities in the wall thickness and dielectric constant. We consider uniform walls and perform imaging using wideband beamforming, with the antennas placed against the wall. Behind-the-wall images are obtained using different structures of transmit and receive arrays. For each array structure, a trajectory of the shifts in the target locations is generated assuming different wall parameters. The target position is estimated as the intersection of the corresponding trajectories. The paper shows that for unknown wall thickness or dielectric constant, the point of intersection is the true target position. In the case when both parameters are unknown, the estimated target location is in close proximity to the target true position. It is demonstrated that the performance of the proposed technique is rather insensitive to the target location behind the wall and to various array structures.**

Manuscript received October 29, 2004; revised March 29, 2005; released for publication August 12, 2005.

IEEE Log No. T-AES/42/1/862554.

Refereeing of this contribution was handled by V. C. Chen.

This work is supported by DARPA under grant MDA972-02-1-0022 and in part by ONR grant N00014-98-1-0176. The content of the information does not necessarily reflect the position or the policy of the Government, and no official endorsement should be inferred.

Authors' address: Center for Advanced Communications, College of Engineering, Villanova University, Villanova, PA 19085, E-mail: (genyuan.wang@villanova.edu).

0018-9251/06/\$17.00 © 2006 IEEE

## I. INTRODUCTION

“Seeing” through obstacles such as walls, doors, and other visually opaque materials using microwave signals is considered as a powerful tool for a variety of applications in both military and commercial paradigms. Through-the-wall imaging (TWI) has been recently sought out in rescue missions, behind-the-wall target detection, surveillance, and reconnaissance. There are several studies on TWI to detect the presence of persons behind walls and track their movements with known wall parameters, such as wall thickness and dielectric constant [1–14]. Ferris and Currie [1] have reviewed existing microwave systems that can detect the presence of persons behind walls and track their movement. Most of the existing systems provided low two dimensional resolutions [2–9]. To improve the resolution, sensor network and coarrays were proposed in references [11], [13, 14], and [23–24], respectively. In practical situations, however, the wall parameters are not known a priori, and need to be properly estimated, so that undistorted, high quality imaging can be obtained. Larger errors in wall parameters cause smearing of the image and displace targets away from their true positions. These effects reduce the accuracy of the TWI and compromise the integrity and main objectives of the system.

The degree of smearing and blurriness of targets can be measured and corrected by applying auto-focusing metrics [17–19], which include normalized sum of image intensity, normalized sum of squared intensity, image entropy, and ratio of standard deviation to mean amplitude. Although these metrics provide maximum, or minimum, values at the correct wall parameters, they are not highly sensitive to reasonable error values. Further, the associated nonconvex error function renders the application of gradient search techniques for the minimum error value nonapplicable.

The errors in wall parameters impact the imaged target position more than its intensity profile. The shifts of targets away from their true positions depend on the errors in the wall parameters as well as the target locations with respect to the antenna array. In this paper, the effect of wall parameter errors on imaging is delineated. We introduce a new approach to locate the target without the knowledge or accurate measurement of the wall parameters. The wall is assumed to be single and uniform. The transmit and receive arrays are assumed to have already been designed to meet the angle resolution specified by the system. Both arrays can be placed against the wall or at a standoff distance. A wideband pulse, meeting the required range resolution, is emitted by the transmit antennas and coherently combined at the receive antennas, using different sets of focusing delays corresponding to different image pixels.

The proposed approach requires imaging to be performed under at least two different array structures, which could simply amount to shifting one or a few antennas, in the transmit or receive array, to new locations. For each array structure, imaging through the wall is obtained using multiple sets of assumed wall parameters. For each set, a trajectory, tracing the bias in the target location, is formed. The intersection of the trajectories, corresponding to the different array structures, is used as the estimate of the true target location.

The organization of rest of this paper is as follows. We provide in Section II the basic theory and equations of the wide-band through the wall imaging. The effect of wall parameter ambiguities on target displacement is discussed in Section III. In Section IV, a target location estimation approach based on the use of two or more array structures is proposed. Simulation results are presented in Section V. The conclusion is provided in Section VI.

## II. FUNDAMENTALS OF THROUGH THE WALL IMAGING

Consider a single transmitter and a single receiver subarray, used to synthesize an  $M$ -element transmit and an  $N$ -element receive linear array, with known locations. The region to be imaged is located along the positive  $z$ -axis. Let the transmitter, placed at the  $m$ th transmit location  $\mathbf{x}_{t_m} = (x_{t_m}, z_{t_m})$ , illuminate the scene with a wideband signal  $s(t)$ . The reflection by any target located in the region being imaged is collected at the  $n$ th receiver located at  $\mathbf{x}_{r_n} = (x_{r_n}, z_{r_n})$ . For the case of a single point target located at  $\mathbf{x}_p = (x_p, z_p) = (R_p \sin \theta_p, R_p \cos \theta_p)$ , the output of the  $n$ th receiver is given by

$$y_{mn}(\mathbf{x}_p) = a(\mathbf{x}_p)s(t - \tau_{p,mn}) \quad (1)$$

where  $a(\mathbf{x}_p)$  is the complex reflectivity of the point target. The wideband signal  $s(t)$  is a narrow pulse that provides the desired range resolution. As shown in Fig. 1, the propagation delay  $\tau_{p,mn}$ , encountered by the signal as it travels from the  $m$ th transmitter to the target located at  $\mathbf{x}_p$ , and back to the  $n$ th receiver, is given by

$$\tau_{p,mn} = \frac{r_{m,p,\text{air}} + l_{n,p,\text{air}}}{c} + \frac{r_{m,p,\text{wall}} + l_{n,p,\text{wall}}}{v} \quad (2)$$

where  $c$  is the speed of light for traveling in the air, and  $v$  is the speed of the wave traveling in the material (wall) with a dielectric constant  $\epsilon$ . In this paper  $\epsilon = 9$  is considered, which corresponds to a concrete wall [12]. The dielectric constant for other types of walls can be found at [20]. We note that  $v = c/\sqrt{\epsilon}$  [12]. The variables  $r_{m,p,\text{air}}$  and  $r_{m,p,\text{wall}}$  represent the traveling distances of the electrical wave in the air and wall, respectively, from the  $m$ th transmitter to the target  $p$ , whereas  $l_{n,p,\text{air}}$  and  $l_{n,p,\text{wall}}$

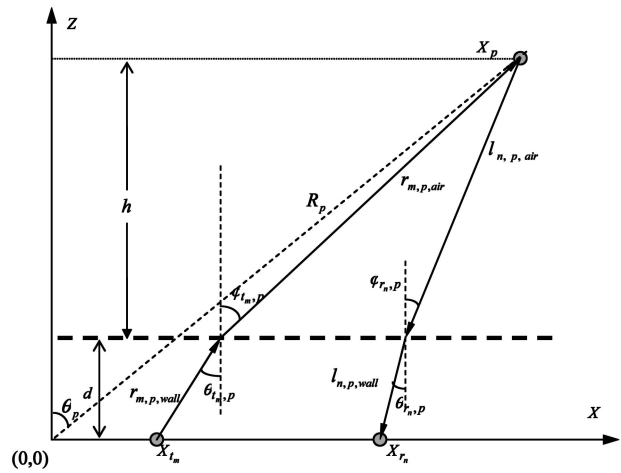


Fig. 1. Geometry for computing distances on receive.

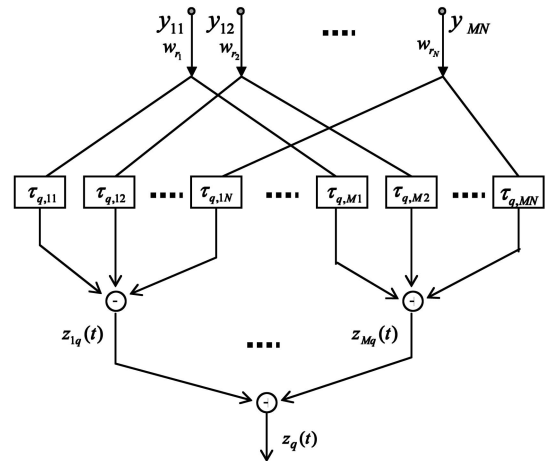


Fig. 2. Block diagram of post-data acquisition beamformer.

are the traveling distances of the wave in the air and wall, respectively, from the target  $p$  to the  $n$ th receiver. The traveling distances inside and outside the wall, and subsequently, the delay in (2), can be precisely computed, given the exact knowledge of the wall parameters [13, 14].

The process, described by (1) and (2), is repeated with the transmitter at the  $m$ th location until all the  $N$  receive locations have been used sequentially. The corresponding  $N$  outputs are processed as follows. The region of interest is divided into a finite number of pixels in range and angle. The complex composite signal corresponding to the image of the pixel located at  $\mathbf{x}_q$  (at range  $R_q$  in the direction  $\theta_q$ ), is obtained by applying time delays and weights to the data at the  $N$  receivers, and summing the results. The corresponding imaging system is shown in Fig. 2. For a single target case, the system output is given by

$$z_{mq}(t) = \sum_{n=1}^N w_{rn} a(\mathbf{x}_p) s(t - \tau_{p,mn} + \tau_{q,mn}) \quad (3)$$

where  $w_{rn}$  is the weight applied to the output of the  $n$ th receiver. The focusing delay  $\tau_{q,mn}$  is applied to the output of the  $n$ th receiver when the transmitter is at the  $m$ th location. This delay, which is given by

$$\tau_{q,mn} = \frac{r_{m,q,\text{air}} + l_{n,q,\text{air}}}{c} + \frac{r_{m,q,\text{wall}} + l_{n,q,\text{wall}}}{v} \quad (4)$$

synchronizes the arrivals at different receive locations for the same pixel, and as such allows coherent imaging of the scene. The variables in (4) are the same as those in (2), except the target pixel  $p$  is replaced by the focusing pixel  $q$ . If  $\mathbf{x}_p = \mathbf{x}_q$ , then the focusing delay  $\tau_{q,mn}$  becomes equal to the target propagation delay  $\tau_{p,mn}$ . In this case, all signals in (3) are coherently combined at pixel  $\mathbf{x}_p = \mathbf{x}_q$ . If  $\mathbf{x}_p \neq \mathbf{x}_q$ , the focusing delay differs from the propagation delay, and the signals in (3) are incoherently combined. In essence, the above coherent and noncoherent combining of target returns is equivalent to forming a beam at pixel  $\mathbf{x}_p$  in range and angle directions. The range resolution can be enhanced by using a larger bandwidth pulse, whereas the angular resolution can be improved by increasing the transmit or/and the receive array apertures.

The above process is repeated by sequential use of the  $M$  transmit locations and produces  $M$  complex composite signals,  $z_{mq}(t)$ ,  $m = 1, 2, \dots, M$ , corresponding to the image of the pixel at  $\mathbf{x}_q$ . The final complex signal corresponding to the pixel located at  $\mathbf{x}_q$  is obtained by the coherent weighted linear combination

$$z_q(t) = \sum_{m=1}^M w_{im} z_{mq}(t) = \sum_{m=1}^M \sum_{n=1}^N w_{im} w_{rn} a(\mathbf{x}_p) s(t - \tau_{p,mn} + \tau_{q,mn}) \quad (5)$$

where  $w_{im}$  is the weight applied to the component signal  $z_{mq}(t)$  obtained using the  $m$ th transmitter. Unlike the focusing delays, the weights  $w_{rn}$  and  $w_{im}$  are independent of the pixel location  $\mathbf{x}_q$ , and serve to define the system point spread function according to desired specifications. The complex amplitude image value for the pixel located at  $\mathbf{x}_q$  is obtained by passing the signal  $z_q(t)$  through a filter matched to the transmitted pulse and sampling the output of the filter at time  $t = 0$ ,

$$I(\mathbf{x}_q) = (z_q(t) * h(t))|_{t=0} \quad (6)$$

where  $h(t) = s^*(-t)$  is the impulse response of the matched filter. The process described by (3)–(6) is performed for all pixels in the region of interest to generate the composite image of the scene. The general case of multiple targets can be obtained by superposition of target reflections. For a wave, traveling from wall material with dielectric constant  $\epsilon$  to air with dielectric constant  $\epsilon_2 = 1$  and incident at an

angle  $\theta$ , the angle of refraction  $\varphi$  is given by Snell's law,

$$\sin \varphi = \sqrt{\epsilon} \sin \theta. \quad (7)$$

The loss of signal power, changing in propagation speed, and the bending effect of the wave as it propagates through and out of a dielectric medium are important factors that must be taken into account for reliable and accurate imaging. Failure to do so would result in errors in the focusing delays for a designated pixel which, in turn, cause errors in determining the locations of the targets.

### III. EFFECT OF WALL PARAMETER AMBIGUITIES

In practical situations, the values of the wall parameters are not exactly known. Below, we discuss the effects of wall parameter ambiguities, namely, the wall thickness and dielectric constant, on imaging through the wall. Errors in these two parameters impact the traveling time both inside and outside the wall, and subsequently, lead to corresponding errors in the applied focusing delays for coherent imaging, given by (4). Using estimated, rather than true, values of the wall parameters, (4) changes to

$$\tilde{\tau}_{q,mn} = \frac{\tilde{r}_{m,q,\text{air}} + \tilde{l}_{n,q,\text{air}}}{c} + \frac{\tilde{r}_{m,q,\text{wall}} + \tilde{l}_{n,q,\text{wall}}}{\tilde{v}} \quad (8)$$

where  $\tilde{v} = c/n\tilde{\epsilon}_e$ ,  $\tilde{r}_{m,q,\text{wall}}$  and  $\tilde{r}_{m,q,\text{air}}$  are the estimated traveling distances of the wave in the wall and air, respectively, from the  $m$ th transmitter to the  $q$  image pixel, whereas  $\tilde{l}_{n,q,\text{wall}}$  and  $\tilde{l}_{n,q,\text{air}}$  are the estimated traveling distances of wave in the wall and air, respectively, from the image pixel  $q$  to the  $n$ th receiver, using estimated wall thickness  $d_e$  and dielectric constant  $\epsilon_e$ . Comparing (4) to (8), it is clear that due to errors in the propagation speed and wave refraction angle,  $\tilde{\tau}_{p,mn} \neq \tau_{p,mn}$ ,  $\tilde{\tau}_{q,mn} \neq \tau_{q,mn}$ . A pure shift in target position due to wall parameter errors will require  $\tilde{\tau}_{q,mn} = \tau_{p,mn}$ ,  $\forall m, n$ , in which case one set of focusing delays in the presence of wall errors must equal to the target propagation delays, given by (2).

#### A. Effect of Wall Thickness Errors

If the estimated, or assumed, wall thickness is  $d_e = d + \Delta d$ , then the time required to travel from the  $m$ th transmit antenna to the  $n$ th receive antenna, reflected at  $p$ , is

$$\tilde{\tau}_{p,mn,d} = \tau_{p,mn} + \Delta \tau_{p,mn,d}. \quad (9)$$

Rewriting (2) as

$$\tau_{p,mn} = \frac{h}{c \cos(\varphi_{im,p})} + \frac{h}{c \cos(\varphi_{rn,p})} + \frac{\sqrt{\epsilon} d}{c \cos(\theta_{im,p})} + \frac{\sqrt{\epsilon} d}{c \cos(\theta_{rn,p})} \quad (10)$$

where  $h = z_p - d$ , then we can obtain

$$\Delta\tau_{p,mn,d} = \frac{\Delta d}{c} \left( \frac{\sin(\varphi_{t_m,p} - \theta_{t_m,p})}{\sin(\theta_{t_m,p})} + \frac{\sin(\varphi_{r_n,p} - \theta_{r_n,p})}{\sin(\theta_{r_n,p})} \right). \quad (11)$$

The derivation of (11) is given in Appendix A. It is clear from the above equation that the change in the time delay is a linear function of  $\Delta d$ , and is a nonlinear function of the incident angles. This implies that the change in the propagation delay is generally antenna dependent. If  $\varepsilon > 1$ , then  $\varphi_{t_m,p} > \theta_{t_m,p}$  and  $\varphi_{r_n,p} > \theta_{r_n,p}$ . It follows from (11) that if the wall thickness is overestimated, i.e.,  $\Delta d > 0$ , then  $\Delta\tau_{p,mn,d} > 0$ . Therefore, when  $d_e$  is larger than the true value  $d$ , the applied focusing delays are greater than those required to coherently combine the signal returns for a target at pixel  $p$ , i.e.,  $\tilde{\tau}_{p,mn} > \tau_{p,mn}$ . Now, consider imaging pixel  $q$  that is closer to the wall than  $p$ , and where there is no target. Under the assumption of wall thickness,  $d_e > d$ , the applied focusing delays are typically greater than those required if there are no wall errors, i.e.,  $d_e = d$ . In this case,  $\tilde{\tau}_{q,mn} > \tau_{q,mn}$ . The above two time delay inequalities suggest that there could be a pixel  $q$  where  $\tilde{\tau}_{q,mn} \approx \tau_{p,mn}$ , rendering a displacement of the target from location  $p$  to location  $q$ . We note that a pure shift in the target position requires  $\tilde{\tau}_{q,mn} = \tau_{p,mn}$ , for all values of  $m$  and  $n$ , otherwise a shift is accompanied with blurriness.

The above argument is illustrated in Fig. 4.

Fig. 4(a) considers three targets at different locations behind the wall. The transmit antennas and receive antennas are symmetric around their center point, and are placed against the wall, as shown in Fig. 3. The transmit array consists of four antennas with inter-element spacing of 0.6 m. The receive array consists of eight antennas with inter-element spacing 0.065 m. Both the transmit and receive arrays are located along the x-axis at positions listed in Table I. The wall thickness is  $d = 0.4$  m and the dielectric constant is  $\varepsilon = 9$ . We use a rectangular pulse with

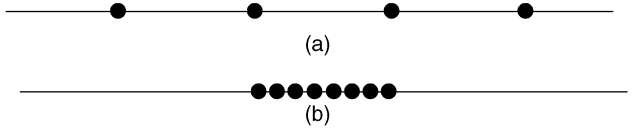


Fig. 3. (a) Transmit array. (b) Receive array.

TABLE I  
Transmit and Receive Array Locations

Element #	1	2	3	4	5	6	7	8
Transmit (m)	-0.9	-0.3	0.3	0.9				
Receive (m)	-0.2625	-0.1875	-0.1125	-0.0375	0.0375	0.1125	0.1875	0.2625

bandwidth 1 GHz and center frequency of 2 GHz. These radar signal characteristics are maintained throughout the paper. The dielectric constant is assumed known, i.e.,  $\varepsilon_e = \varepsilon$ , but the wall thickness is unknown and assumes the values  $d_e = 0.6, 0.4, 0.2$  m. The second value is equal to the true wall thickness, whereas for the other two values,  $d_e \neq d$ . The images corresponding to different pairs of wall parameters  $(\varepsilon, d_e)$  are superimposed. It is evident from Fig. 4(a) that there is no significant changes in imaging qualities, even when the incorrect wall parameters are used. On the other hand, the targets are clearly shifted away from their true positions.

#### B. Effect of Dielectric Constant Errors

Similar to the wall thickness errors, errors in the dielectric constant also impair imaging. If the estimated, or assumed, dielectric constant is  $\varepsilon_e = \varepsilon + \Delta\varepsilon$ , then the corresponding focusing delay becomes

$$\tilde{\tau}_{p,mn,\varepsilon} = \tau_{p,mn} + \Delta\tau_{p,mn,\varepsilon} \quad (12)$$

where

$$\Delta\tau_{p,mn,\varepsilon} = \frac{d\Delta\varepsilon}{2\sqrt{\varepsilon}c} \left( \frac{1}{\cos(\theta_{t_m,p})} + \frac{1}{\cos(\theta_{r_n,p})} \right). \quad (13)$$

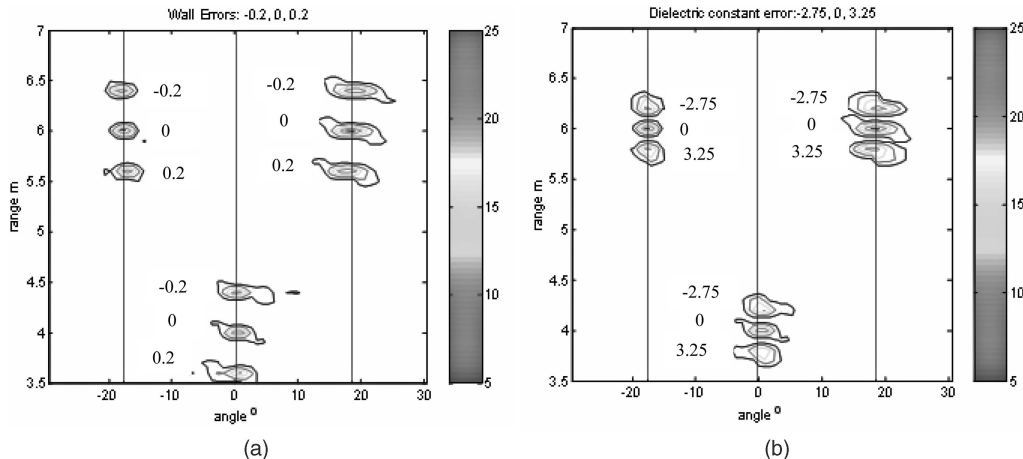


Fig. 4. Changes in imaging for different wall assumptions. (a) Effect of wall thickness errors. (b) Effect of dielectric constant errors.

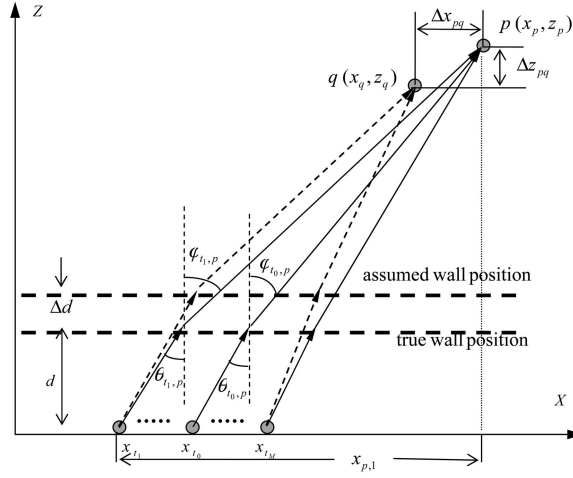


Fig. 5. Geometry for computing imaged position  $q$  corresponding to target  $p$ .

The derivation of (13) is given in Appendix B. It is evident from the above equation that the change in the propagation delay is dependent on  $d$ ,  $\varepsilon$ , and the incident angles. Further, when  $\varepsilon > 1$ , then  $\Delta\tau_{p,mn,\varepsilon} > 0$  for  $\Delta\varepsilon > 0$ . Therefore, if  $\varepsilon_e$  is larger than the true value  $\varepsilon$ , the corresponding speed of signal traveling in the wall  $\tilde{v} < v$ , and  $\tilde{\tau}_{p,mn} > \tau_{p,mn}$ . Similar to the case of  $d_e > d$  discussed in Section IIIA, for  $\varepsilon_e > \varepsilon$ , the target at location  $p$  may be displaced to some pixel  $q$  closer to the wall. For illustration, we consider the same wall characteristics and targets used in Section IIIA. In this case, however, we assume knowledge of the true wall thickness,  $d_e = d$ , but use different values of the wall dielectric constant,  $\varepsilon_e = 6.25, 9, 12.25$ . The second value is equal to the true value of the dielectric constant, whereas for the first and third values,  $\varepsilon_e \neq \varepsilon$ . The images corresponding to different pairs of wall parameters are superimposed in Fig. 4(b). It is evident that the image quality under different assumed values of the dielectric constant are almost the same, but the targets are shifted away from their true positions.

#### IV. NEW APPROACH FOR TARGET LOCATION

Depending on the applications, large target shifts can be undesirable and must be corrected. The shift in the target position depends on the wall parameter errors and the relative position of target with respect to the wall. It is easy to understand the target displacement in range due to wall errors. Below, we consider the effect of the wall parameter errors on targets in angle.

##### A. Shift of Target in the Image Results with Wall Thickness Error

Now, we consider target shifts due to different wall thickness errors. For simplicity of analysis, we focus on the simple case of one way traveling from transmit array to a target  $p$  located at  $(x_p, z_p)$ , where the  $m$ th transmit antenna is located at  $(x_t, 0)$ . In this case, and

as shown in Fig. 5, the traveling time  $\tau_{p,m}$  between the  $m$ th transmit antenna to the target  $p$ , is expressed as

$$\tau_{p,m} = \frac{z_p - d}{c \cos(\varphi_{t_m,p})} + \frac{\sqrt{\varepsilon}d}{c \cos(\theta_{t_m,p})}. \quad (14)$$

Assume that under the wall error  $\Delta d = d_e - d$ , the target, whose true position is  $p$ , appears at point  $q$  at  $(x_q, z_q)$ . Denote  $\Delta x_{pq} = x_q - x_p$  and  $\Delta z_{pq} = z_q - z_p$ . The relationship of  $\Delta x_{pq}$ ,  $\Delta z_{pq}$ , antenna and the target locations is shown in Fig. 5. For small values of  $\Delta d$ , the estimated time delay from the  $m$ th antenna sensor to point  $q$  is expressed as

$$\tilde{\tau}_{q,m} = \tau_{p,m} + \Delta\tau_{pq,m} \quad (15)$$

where

$$\begin{aligned} \Delta\tau_{pq,m} &= \frac{\partial\tau_{pq,m}}{\partial d} \Delta d + \frac{\partial\tau_{pq,m}}{\partial x_q} \Delta x_{pq} + \frac{\partial\tau_{pq,m}}{\partial z_q} \Delta z_{pq} \\ &= \frac{\Delta d \sin(\varphi_{t_m,p} - \theta_{t_m,p})}{c \sin(\theta_{t_m,p})} + \frac{\Delta x_{pq} \sin(\varphi_{t_m,p})}{c} \\ &\quad + \frac{\Delta z_{pq} \cos(\varphi_{t_m,p})}{c}. \end{aligned} \quad (16)$$

Note that  $\partial\tau_{pq,m}/\partial d = \sin(\varphi_{t_m,p} - \theta_{t_m,p})/c \sin(\theta_{t_m,p})$ , obtained from (41), has considered the subsequent change of the incident angles due to the change in  $d$ . In here,  $\partial\tau_{pq,m}/\partial d$  is used to distinguish this operation from  $\partial\tau_{p,m}/\partial d$  operation in (41) which assumes fixed incident angles. For the array antenna to synthesize an image at position  $q$  of a target physically present at location  $p$ , the difference between  $\tilde{\tau}_{q,m}$  and  $\tau_{p,m}$  should ideally be zero for all  $M$  antennas (Note that, theoretically, blurriness will occur if  $\Delta\tau_{pq,m} \neq 0$  for any  $m$ ). To simplify the problem, we assume that the array aperture is small, and consider the following two conditions at the center of the array antenna (it is not necessary that an antenna should exist in the center of the array). First, the time delay  $\tilde{\tau}_{q,0}$  should be equal to  $\tau_{p,0}$ , that is,

$$\Delta\tau_{pq,0} = 0 \quad (17)$$

where the subscript 0 denotes the center of the array. Second, the above time difference is invariant with the antenna, i.e.,

$$\partial\Delta\tau_{pq,0}/\partial\varphi_{t_0,p} = 0. \quad (18)$$

From (16),

$$\begin{aligned} \Delta\tau_{pq,0} &= \frac{\Delta d}{c \sin(\theta_{t_0,p})} [\sin(\varphi_{t_0,p}) \cos(\theta_{t_0,p}) - \sin(\theta_{t_0,p}) \cos(\varphi_{t_0,p})] \\ &\quad + \frac{\Delta x_{pq} \sin(\varphi_{t_0,p})}{c} + \frac{\Delta z_{pq} \cos(\varphi_{t_0,p})}{c} \\ &= \frac{\Delta d}{c} [\sqrt{\varepsilon} \cos(\theta_{t_0,p}) - \cos(\varphi_{t_0,p})] \\ &\quad + \frac{\Delta x_{pq} \sin(\varphi_{t_0,p})}{c} + \frac{\Delta z_{pq} \cos(\varphi_{t_0,p})}{c} \end{aligned} \quad (19)$$

where  $\theta_{t_0,p}$  and  $\varphi_{t_0,p}$ , are respectively, the incident and refraction angles in the wall and air, related to the path from the center of the transmit array to the target  $p$ . Accordingly,

$$\frac{\partial \Delta \tau_{pq,0}}{\partial \varphi_{t_0,p}} = \frac{\Delta d}{c} \left( -\frac{\sin(\theta_{t_0,p}) \cos(\varphi_{t_0,p})}{\cos(\theta_{t_0,p})} + \sin(\varphi_{t_0,p}) \right) + \frac{\Delta x_{pq} \cos(\varphi_{t_0,p})}{c} - \frac{\Delta z_{pq} \sin(\varphi_{t_0,p})}{c}. \quad (20)$$

From (19) and (20), we obtain

$$\Delta x_{pq} = -\Delta d(\varepsilon - 1) \tan(\theta_{t_0,p}) \quad (21)$$

$$\Delta z_{pq} = -\Delta d \left( \frac{\cos(\varphi_{t_0,p})}{\cos(\theta_{t_0,p})} \sqrt{\varepsilon} - 1 \right). \quad (22)$$

From (21) and (22),

$$\frac{\Delta x_{pq}}{\Delta z_{pq}} = \frac{(\varepsilon - 1) \tan(\theta_{t_0,p})}{\frac{\cos(\varphi_{t_0,p})}{\cos(\theta_{t_0,p})} \sqrt{\varepsilon} - 1} = \frac{(\varepsilon - 1) \sin(\theta_{t_0,p})}{\sqrt{\varepsilon} \cos(\varphi_{t_0,p}) - \cos(\theta_{t_0,p})} > \frac{(\varepsilon - 1) \sin(\theta_{t_0,p})}{(\sqrt{\varepsilon} - 1) \cos(\varphi_{t_0,p})} > \tan(\varphi_{t_0,p}). \quad (23)$$

For reasonable values of  $\theta_{t_0,p}$  and  $\varphi_{t_0,p}$ ,

$$\frac{\cos(\varphi_{t_0,p})}{\cos(\theta_{t_0,p})} \sqrt{\varepsilon} - 1 > 0.$$

Therefore, when  $\Delta d$  is positive, both  $\Delta x_{pq}$  and  $\Delta z_{pq}$  are negative, and  $q$  appears closer to the antenna array than  $p$ . Expression (23) also implies that the target moves toward the center of the antenna array when a positive wall thickness error is introduced. We can obtain a similar conclusion for the propagation between the target and the receive array. Therefore, the above equation remains valid when the two way traveling (from transmitter to target and from target to receiver) time is considered. We note that when considering the effect of both the transmit and receive arrays, the shift of the image is given by

$$\Delta x_{pq} = -\Delta d(\varepsilon - 1) [\tan(\theta_{t_0,p}) + \tan(\theta_{r_0,p})] \quad (24)$$

$$\Delta z_{pq} = -\Delta d \left[ \left( \frac{\cos(\varphi_{t_0,p})}{\cos(\theta_{t_0,p})} \sqrt{\varepsilon} - 1 \right) + \left( \frac{\cos(\varphi_{r_0,p})}{\cos(\theta_{r_0,p})} \sqrt{\varepsilon} - 1 \right) \right] \quad (25)$$

where  $\theta_{r_0,p}$  and  $\varphi_{r_0,p}$  are, respectively, the incident and refraction angle in the wall and air related to the path from the target  $p$  to the center of the receive array.

Referring back to Fig. 4(a) and examining the shifting patterns of the targets, we find a distinction between the movements of the center target, located at  $(4,0)$  and the off-center targets located at  $(6, \pi/10)$  and  $(6, -\pi/10)$ . The transmit and receive antenna arrays

are placed against the wall symmetrically at the two sides of  $(4,0)$ . Therefore the antenna array appears at one side of the target  $(6, \pi/10)$  and on the other side of  $(6, -\pi/10)$ . From the above analysis, the center target will not shift to the left or the right, but will only move along the path perpendicular to the wall, which is the case in Fig. 4(a). Based on the analytical results, the off-center targets will move toward the center of the antenna array, which is verified by the simulation result in Fig. 4(a), which shows that the images of targets located at  $\pi/10$  and  $-\pi/10$  shift, not only in range but also in angle. When the assumed wall thickness is larger than its true value, the targets at  $\pi/10$  and  $-\pi/10$  move close to the wall and also toward the center view angle, 0.

The above example demonstrates that the imaged target displacements depend on the target relative position to the transmit and receive arrays. Accordingly, two different array structures will yield two different displacement patterns. Based on this property, we propose, below, a scheme to estimate the target true position by performing imaging with different locations of the transmit arrays.

## B. One Parameter is Unknown

In this section, we propose a scheme to estimate the true positions of targets as well as the wall parameter when only one of the two wall parameters, i.e., wall thickness or wall dielectric constant, is known. First, we consider the case where only the dielectric constant is known. The transmit and receive arrays are placed as shown in Fig. 3 and Table I. By using several assumed values of the wall thickness, a series of shifted target images can be generated. The target shifts toward to or away from the wall, resulting in a shifting pattern that depends on the array structure. The connection of the centers of the same imaged target forms the target displacement trajectory. The target trajectories corresponding to different array structures intersect at the true target position. The corresponding value of the assumed wall thickness at that position is its true value. Figs. 6(a) and 7(a) show the simulation results of a target located at  $R_p = 6$  m,  $\theta_p = \pi/10 = 18^\circ$ , with known dielectric constant and different assumed wall thickness values. Fig. 6(a) demonstrates the change in angle, whereas Fig. 7(a) demonstrates the change in range. In both figures, the true position of the target is marked "o". When the wall thickness has negative errors, i.e.,  $d_e < d$ , the target is imaged at  $(R_q, \theta_q)$ , with  $R_q > 6$  and  $\theta_q > 18^\circ$ . When  $d_e = d$ , the target is imaged at its true position with distance 6 m and view angle  $18^\circ$ , i.e.,  $(R_q, \theta_q) = (R_p, \theta_p) = (6, \pi/10)$ . On the other hand, if  $d_e > d$ , then  $R_q < 6$  and  $\theta_q < 18^\circ$ , and the target image moves to the lower left side of its true position. This is consistent with the analysis given in Section IVA. As the assumed wall thickness changes from small to

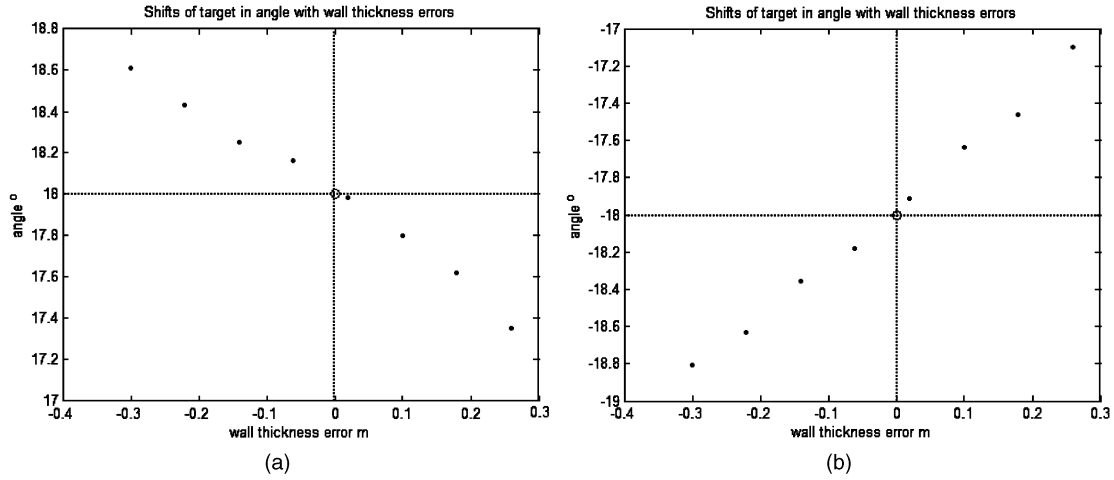


Fig. 6. Shifts of target in angle with wall thickness errors. (a) Target at  $(6, \pi/10)$ . (b) Target at  $(6, -\pi/10)$ .

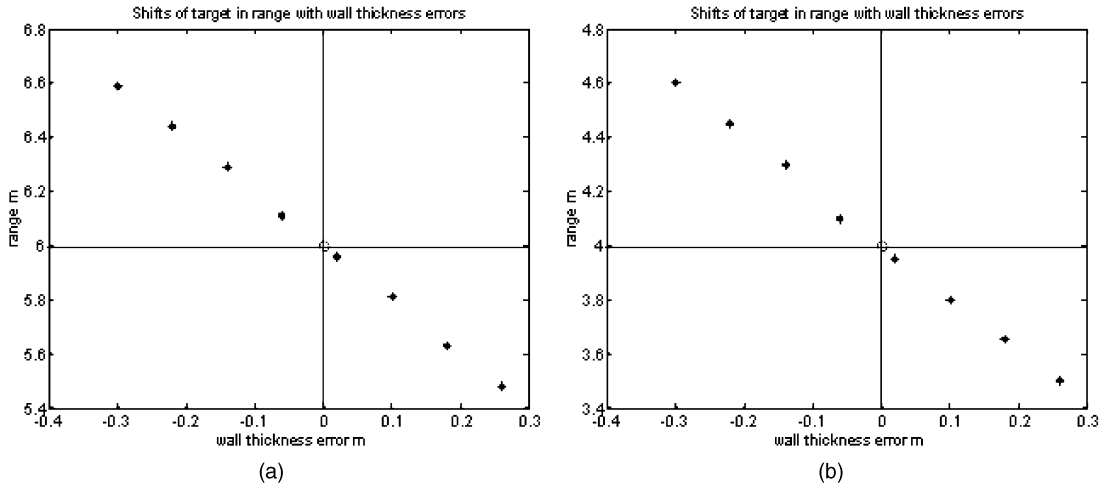


Fig. 7. Shifts of target in range with wall thickness errors. (a) Target at  $(6, \pi/10)$ . (b) Target at  $(4, 0^\circ)$ .

large, the trajectory of the target images crosses over the target true position. Similar pattern of behavior is obtained for the second target located at  $(6, -\pi/10)$  and depicted in Fig. 6(b), which is the counterpart of Fig 6(a). However, in Fig. 6(b), unlike the first target, when the wall thickness error is negative, the target is displaced to the upper left side, instead of the upper right side, of the target's true position. In essence, for both targets, the view angle increases in absolute value for reduced wall thickness estimate, depicting a move towards the sides and away from the center. Fig. 7(b) shows the shift in range for the target at  $(4, 0)$ . When the wall thickness error is negative, the target images move away from the wall, causing an increase in range.

Next, we modify the antenna array structure by moving the transmit array 0.8 m along the x axis, and generate another series of images. The images of targets follow the same moving pattern as in the original structure. However, because of the different locations of the transmit antennas in the two array structures, the respective target displacement

trajectories are not identical. The intersection of the two trajectories provides the true target position and the true wall thickness. This is demonstrated by the simulation results shown in Fig. 8(a). In this figure, “.” indicates the target image positions in angles for the original transmit array structure, whereas “\*” indicates the target image positions in angles for the shifted transmit array structure.

Below, we give a pseudocode of the proposed target location estimation algorithm with known dielectric constant,  $\varepsilon$ .

1) Generate a series of images  $A_{d_{e1}}, A_{d_{e2}}, \dots, A_{d_{ek}}$ , for a given array structure, and using  $\varepsilon_e = \varepsilon$ . These images correspond to the assumed wall thickness values  $d_{e1}, d_{e2}, \dots, d_{ek}$ .

2) Find the position  $I_1(x, z, d_{e_l})$  in  $x$ - $z$  plane of the target  $p$  in image  $A_{d_{e_l}}$  for  $1 \leq l \leq k$ .

3) Fit  $I_1(x, z, d_{e_l})$   $1 \leq l \leq k$  with two separate polynomials  $z = f_1(x)$ ,  $u = g_1(z)$  of orders  $r_1$  and  $\tilde{r}_1$ , respectively, where  $u$  represents the variable of wall thickness.

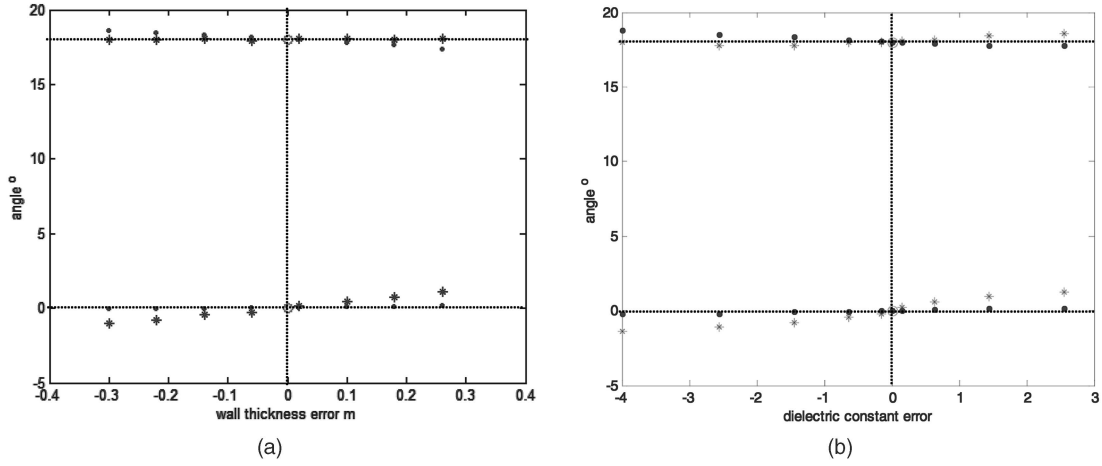


Fig. 8. Target position and other wall parameter estimation with one parameter known. (a) Dielectric constant is known. (b) Wall thickness is known.

4) Repeat step 1 and generate another series of images  $B_{d_{e_1}}, B_{d_{e_2}}, \dots, B_{d_{e_k}}$ , using another array structure, and  $\varepsilon_e = \varepsilon$ .

5) Find the position  $I_2(x, z, d_{e_l})$  in  $x$ - $z$  plane for the same target  $p$  in image  $B_{d_{e_l}}$  for  $1 \leq l \leq k$ .

6) Fit  $I_2(x, z, d_{e_l})$   $1 \leq l \leq k$  with two polynomials  $z = f_2(x)$ ,  $u = g_2(z)$  of orders  $r_2$  and  $\tilde{r}_2$ , respectively.

7) Find the cross point  $(x_0, z_0)$  of  $z = f_2(x)$  and  $z = f_1(x)$ , i.e.,  $z_0 = f_2(x_0) = f_1(x_0)$ .

8) Let  $\hat{d} = \frac{1}{2}(g_1(z_0) + g_2(z_0))$  as the estimated wall thickness.

9) Use the wall parameter  $(\varepsilon, \hat{d})$  to generate the final image.

The above argument and experiment can be extended to the case when the true wall thickness is known, but the dielectric constant is unknown. Trajectories, similar to those shown for the unknown wall thickness case, can be generated with respective figures with close similarities to their counterparts in Figs. 6 and 7. We, therefore, omit the detailed presentation for the known wall thickness case. Fig. 8(b) shows the simulation results of the two trajectories and their intersection point for this case.

### C. Both Parameters are Unknown

Now, we consider the case where both the wall thickness and the dielectric constant are unknown. We first assume a value of one of the two parameters, say the dielectric constant,  $\varepsilon_e$ . Then, we proceed with the same steps used in Section IVB, where the dielectric constant is known. That is, we generate a sequence of images using different assumed values of the wall thickness. Since  $\varepsilon_e$  has an error, the trajectory, unlike the previous case, will not be guaranteed to crossover the true target position. However, the same pattern under the correct dielectric constant  $\varepsilon$  persists; the

images move closer to the center of the antenna array when a series of assumed wall thickness  $d_{e_1} < d_{e_2} < \dots < d_{e_l}$  are used.

To analytically address the above imaging problem, we estimate the displacement of the image in the  $x$ -direction when there is an error in the dielectric constant, and  $\Delta d$  is such that the target position in the  $z$ -direction is unchanged. That is, the target located at point  $p$ ,  $(x_p, z_p)$ , is imaged at the point  $q$  located at  $(x_q, z_q)$ , where  $z_p = z_q$ , but  $x_p$  and  $x_q$  may or may not be equal. The analysis and simulation below show, that for  $\Delta z = 0$ , the displacement in the  $x$ -direction  $\Delta x_{pq} = x_q - x_p$  assumes very small values.

Denote  $\Delta d = d_e - d$  and  $\Delta \varepsilon = \varepsilon_e - \varepsilon$ . When  $\Delta \varepsilon$  is small, the time delay from the  $m$ th antenna to point  $q$  is expressed as

$$\tilde{\tau}_{q,m} = \tau_{p,m} + \Delta \tau_{pq,m} \quad (26)$$

where

$$\begin{aligned} \Delta \tau_{pq,m} &= \frac{\partial \tau_{pq,m}}{\partial d} \Delta d + \frac{\partial \tau_{pq,m}}{\partial \varepsilon} \Delta \varepsilon + \frac{\partial \tau_{pq,m}}{\partial x_{pq}} \Delta x_{pq} \\ &= \frac{\Delta d \sin(\varphi_{t_m,p} - \theta_{t_m,p})}{c \sin(\theta_{t_m,p})} + \frac{\Delta \varepsilon d}{2\sqrt{\varepsilon}c \cos(\theta_{t_m,p})} \\ &\quad + \frac{\Delta x_{pq} \sin(\varphi_{t_m,p})}{c}. \end{aligned} \quad (27)$$

Similar to the derivation in Section IVA, we assume that the array aperture is small, and the two conditions embodied in (17) and (18) at the center of the antenna array should be satisfied, where  $\Delta \tau_{pq,m}$  is now given by (27). In this case,

$$\begin{aligned} \Delta \tau_{pq,0} &= \frac{\Delta d \sin(\varphi_{t_0,p} - \theta_{t_0,p})}{c \sin(\theta_{t_0,p})} + \frac{\Delta \varepsilon d}{2\sqrt{\varepsilon}c \cos(\theta_{t_0,p})} \\ &\quad + \frac{\Delta x_{pq} \sin(\varphi_{t_0,p})}{c} = 0 \end{aligned} \quad (28)$$

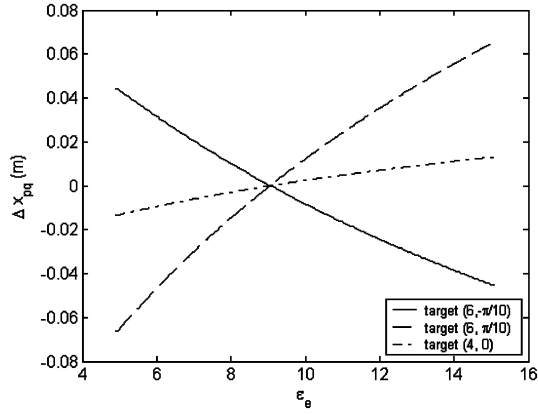


Fig. 9. Displacement of targets.

and

$$\begin{aligned} \frac{\partial \Delta \tau_{q,0}}{\partial \varphi_{t_0,q}} &= \frac{\Delta d}{c} \left( -\frac{\sin(\theta_{t_0,q}) \cos(\varphi_{t_0,q})}{\cos(\theta_{t_0,q})} + \sin(\varphi_{t_0,q}) \right) \\ &+ \frac{\Delta \varepsilon d \sin(\theta_{t_0,q}) \cos(\varphi_{t_0,q})}{2\sqrt{\varepsilon} c \cos^3(\theta_{t_0,q})} \\ &+ \frac{\Delta x_{pq} \cos(\varphi_{t_0,q})}{c} = 0. \end{aligned} \quad (29)$$

From (28) and (29), we obtain

$$\Delta x_{pq} = -\Delta \varepsilon \frac{d \sin(\varphi_{t_0,p} - \theta_{t_0,p})}{2\varepsilon \cos^2(\theta_{t_0,p}) \cos(\varphi_{t_0,p} + \theta_{t_0,p})}. \quad (30)$$

The corresponding  $\Delta d$  is given by

$$\Delta d = -\Delta \varepsilon \frac{d \sin(\theta_{t_0,p}) \cos(\varphi_{t_0,p}) \cos(2\theta_{t_0,p})}{2\sqrt{\varepsilon} \sin(\varphi_{t_0,p} - \theta_{t_0,p}) \cos^2(\theta_{t_0,p}) \cos(\varphi_{t_0,p} + \theta_{t_0,p})}. \quad (31)$$

Because the relationship between  $\Delta x_{pq}$  and  $\Delta \varepsilon$  is not linear, for a relatively large value of  $\Delta \varepsilon$ , we can obtain a more accurate approximation of  $\Delta x_{pq}$  through

the following integral,

$$\begin{aligned} \Delta x_{pq} &= -\int_{\varepsilon}^{\varepsilon+\Delta \varepsilon} \frac{d \sin(\varphi_{t_0,p} - \theta_{t_0,p})}{2\varepsilon \cos^2(\varphi_{t_0,p}) \cos(\varphi_{t_0,p} + \theta_{t_0,p})} d\varepsilon \\ &= -\frac{d \sin(\varphi_{t_0,p} - \theta_{t_0,p})}{\cos^2(\varphi_{t_0,p}) \cos(\varphi_{t_0,p} + \theta_{t_0,p})} \ln \sqrt{\frac{\varepsilon + \Delta \varepsilon}{\varepsilon}}. \end{aligned} \quad (32)$$

The result of (32) is illustrated in Fig. 9 for the three targets used in Fig. 4, i.e.,  $(x_p, z_p) = (6 \sin(\pi/10), 6 \cos(\pi/10))$ ,  $(6 \sin(-\pi/10), 6 \cos(-\pi/10))$ ,  $(0, 4)$ , where  $\varepsilon_e$  varies from 5 to 15. The true wall thickness is 0.4 m and the true dielectric constant is 9. The array geometry is explained in Table I. The center of the transmit array is shifted to the left by 0.6 m, i.e.,  $(x_{t_0}, z_{t_0}) = (-0.6, 0)$ , whereas the receive array is located at the center point, i.e.,  $(x_{r_0}, z_{r_0}) = (0, 0)$ . The results in Fig. 9 have considered the target displacement caused by using all antennas. It can be seen that the displacement is very small and is considered negligible compared with the imaging resolution. Therefore, for all practical purposes, it is accurate to assume that the imaged target passes through its true position, even though an incorrect dielectric constant is used.

The above analysis is verified by the simulation example depicted in Fig. 10. The transmit array used in Fig. 10 is that of Table I with the center of array shifted  $-0.6$  m along x-axis. The locations of three targets as well as the wall parameters are exactly the same as those used in Fig. 6. We set  $\varepsilon_e = 6.25$ . Six different assumed wall thickness values are used to generate the displacement trajectory, namely,  $\Delta d = -0.3, -0.2, -0.1, 0.1, 0.2, 0.3$ .

To compare the moving patterns of  $\varepsilon_e = 6.25$  and  $\varepsilon_e = \varepsilon = 9$ , the images of Fig. 10 are superimposed, in Fig. 11 with the results obtained from using the exact dielectric constant, and the same set of wall thickness errors. Fig. 10(a) and Fig. 11(a) show that the image trajectories of each target are merged. The

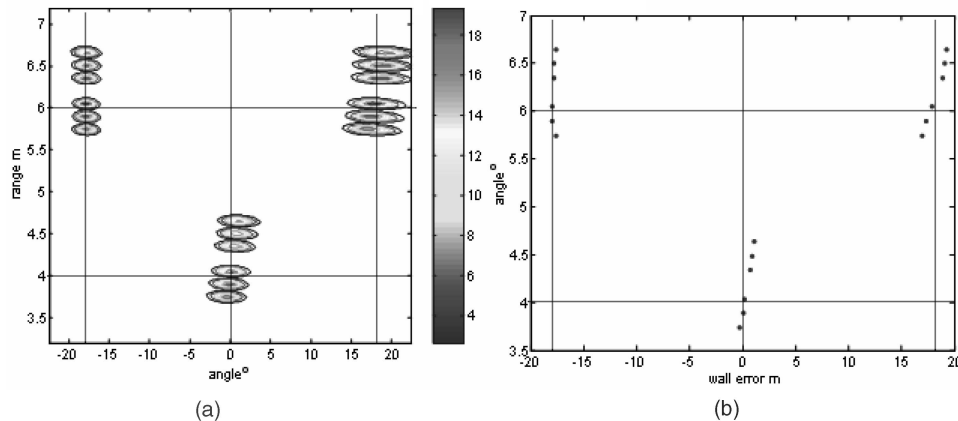


Fig. 10. Displacement trajectory with different assumed wall thickness and  $\varepsilon_e = 6.25$  for  $\varepsilon = 9$ , center of transmit array shifted by  $-0.6$  m from Table I. (a) Images with  $\varepsilon_e = 6.25$  and different  $d_e$ . (b) Peaks of images with  $\varepsilon_e = 6.25$  and different  $d_e$ .

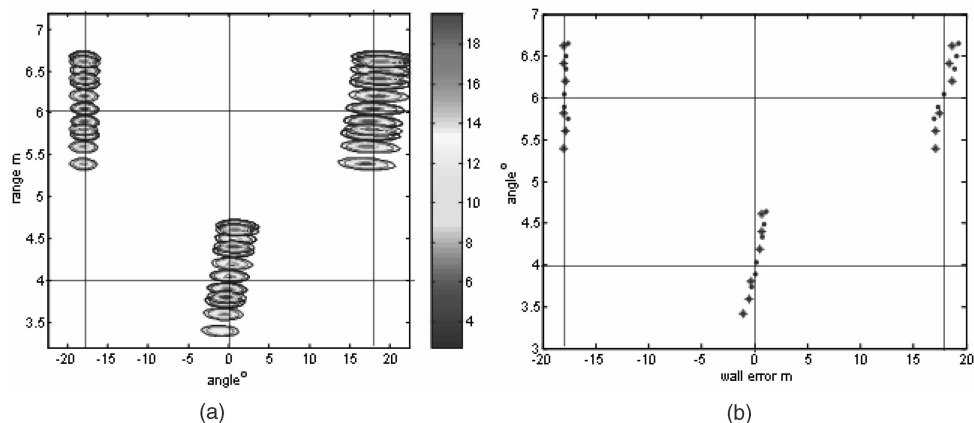


Fig. 11. Superimposed images in Fig. 10 with  $\varepsilon_e = 6.25$  and those  $\varepsilon_e = \varepsilon = 9$  and different assumed wall thickness  $d_e$ . (a) Images with  $\varepsilon_e = 6.25$ ,  $\varepsilon_e = 9$ , and different  $d_e$ . (b) Peaks of images with  $\varepsilon_e = 6.25$ ,  $\varepsilon_e = 9$  and different  $d_e$ .

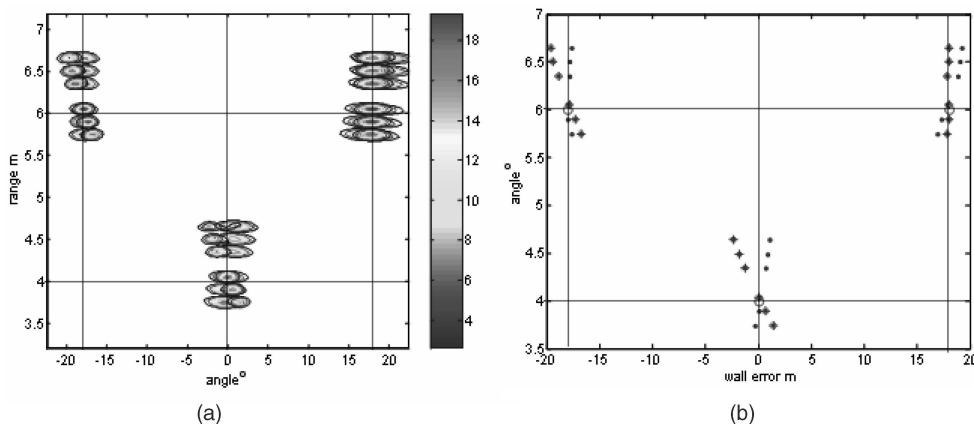


Fig. 12. Finding true image with estimated wall parameters using  $\varepsilon_e = 6.25$ . (a) Images with  $\varepsilon_e$  and different  $d_e$ . (b) Peaks of images with  $\varepsilon_e$  and different  $d_e$ .

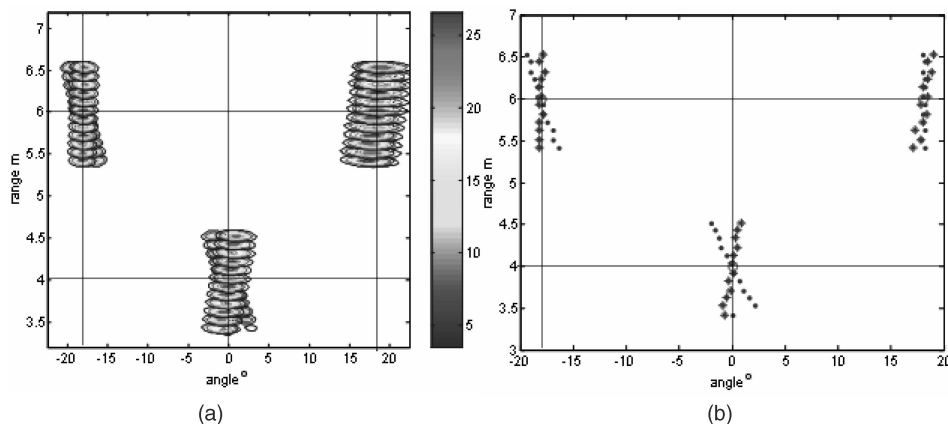


Fig. 13. Finding true image with estimated wall parameters using  $\varepsilon_e = 12.25$ . (a) Images with  $\varepsilon_e$  and different  $d_e$ . (b) Peaks of images with  $\varepsilon_e$  and different  $d_e$ .

peak points of images with  $\varepsilon_e = 6.25$  and  $\varepsilon_e = \varepsilon = 9$  are plotted with “.” and “\*”, respectively in Fig. 11(b). The target trajectories are almost the same. A very slight difference is noticed in Fig. 11(b).

To estimate the position of targets, an array with a different structure is added. The receive array in the new structure is the same as that used in Figs. 10

and 11. The transmit array used in the new structure, however, is that of Table I with a 0.6 m shift along the x-axis, i.e., the transmit arrays in the two structures are shifted 0.6 m to the left and to the right from the original structure given in Table I. Using this new array and the same values of  $\varepsilon_e$  and  $d_e$  in Fig. 10, we generate another series of images. The images

with the new array structure and those of Fig. 10(a) are superimposed in Fig. 12(a). The corresponding peak points of the images are plotted in Fig. 12(b). Fig. 12 shows that the cross points of the image trajectories are almost at the true positions of the respected targets, which are marked with “o”. Note that, because of the small array apertures, the angle resolution of the image is limited.

Another example is shown in Fig. 13, where all the parameters are the same as those in Fig. 12, but  $\varepsilon_e = 12.25$  is assumed. Unlike Fig. 12, the assumed dielectric constant in Fig. 13 has a positive error. Comparing with those in Fig. 12, the images in Fig. 13 move closer to the antenna arrays. However, similar to the results in Fig. 12, the cross point of the image trajectories of each target well coincides with its true position.

Similar to the pseudocode for the case with one known wall parameter, we can provide a pseudocode for the underlying case where both wall parameters are unknown. We fix the value of the dielectric constant  $\varepsilon_e$  and generate different image series with different assumed wall thickness  $d_{e_1}, d_{e_2}, \dots, d_{e_k}$  and under two different array structures.

- 1) Generate a series of images  $A_{d_{e_1}}, A_{d_{e_2}}, \dots, A_{d_{e_k}}$ , using one array structure and an estimated dielectric constant value  $\varepsilon_e$ . These images correspond to assumed wall thickness  $d_{e_1}, d_{e_2}, \dots, d_{e_k}$ .
- 2) Find the position  $I_1(x, z, d_{e_l})$  in  $x$ - $z$  plane of a target  $p$  in image  $A_{d_{e_l}}$  for  $1 \leq l \leq k$ .
- 3) Fit  $I_1(x, z, d_{e_l})$   $1 \leq l \leq k$  with two polynomials  $z = f_1(x)$  and  $u = g_1(z)$  of orders  $r_1$  and  $\tilde{r}_1$  respectively, where  $u$  represents the variable of wall thickness.
- 4) Repeat step 1 and generate an image series  $B_{d_{e_1}}, B_{d_{e_2}}, \dots, B_{d_{e_k}}$ , using another array structure.
- 5) Find the position  $I_2(x, z, d_{e_l})$  in  $x$ - $z$  plane for the same target  $p$  used in image  $A_{d_{e_l}}$  for  $1 \leq l \leq k$ .
- 6) Fit  $I_2(x, z, d_{e_l})$   $1 \leq l \leq k$  with two polynomials  $z = f_2(x)$  and  $u = g_2(z)$  of orders  $r_2$  and  $\tilde{r}_2$ , respectively.
- 7) Find the cross point  $(x_0, z_0)$  of  $z = f_2(x)$  and  $z = f_1(x)$ , i.e.,  $z_0 = f_2(x_0) = f_1(x_0)$ .
- 8) Use  $\hat{d}_0 = \frac{1}{2}(g_1(z_0) + g_2(z_0))$  as the estimated wall thickness.
- 9) Use the wall parameter  $(\varepsilon_e, \hat{d}_0)$  to generate the final image.

Notice that the estimated  $\hat{d}_0$  in step 8 depends on the assumed dielectric constant  $\varepsilon_e$ . Therefore, the pair  $(\varepsilon_e, \hat{d}_0)$  employed to generate the final image is not unique.

## V. SIMULATION RESULTS

In addition to the examples provided in the previous sections, we consider in this section the case

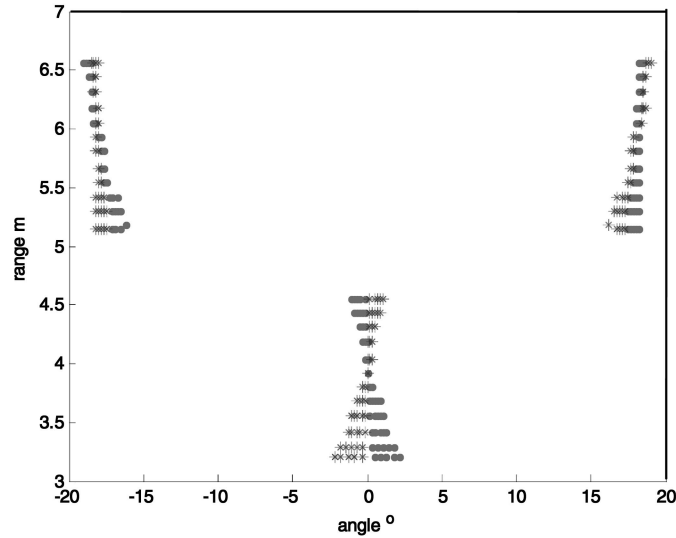
where both wall parameters are unknown. From the discussions in Section IVC, there exist different pairs of  $(\varepsilon_e, d_e)$  that can be used such that the targets are imaged at their correct positions. For illustration, we consider three targets located at  $(4, 0)$ ,  $(6, \pi/10)$  and  $(6, -\pi/10)$  with wall parameters  $\varepsilon = 9$ ,  $d = 0.4$  m. The transmit and receive arrays are the same as those used in Fig. 13.

First we show that the target images pass through their “true” positions, even though the assumed wall parameters have errors. Figs. 14(a) and 14(b) show the results with fixed assumed dielectric constant  $\varepsilon_e = 12.25$  and  $\varepsilon_e = 6.25$  with 12 different assumed values of wall thickness  $d_e$  with  $d - d_e = 0.25, 0.20, 0.15, 0.10, 0.05, 0, -0.05, -0.1, -0.15, -0.20, -0.25, -0.3$  m. The transmit array is shifted in the  $x$ -direction by  $-0.5, -0.4, -0.3, -0.2, -0.1, 0.1, 0.2, 0.3, 0.4, 0.5$  m from its original position in Table I. The positions of images obtained by the transmit array with a positive shift are marked by “\*”, whereas those obtained by the transmit array with a negative shift are marked by “.”. Fig. 14 shows that targets cross at their true positions.

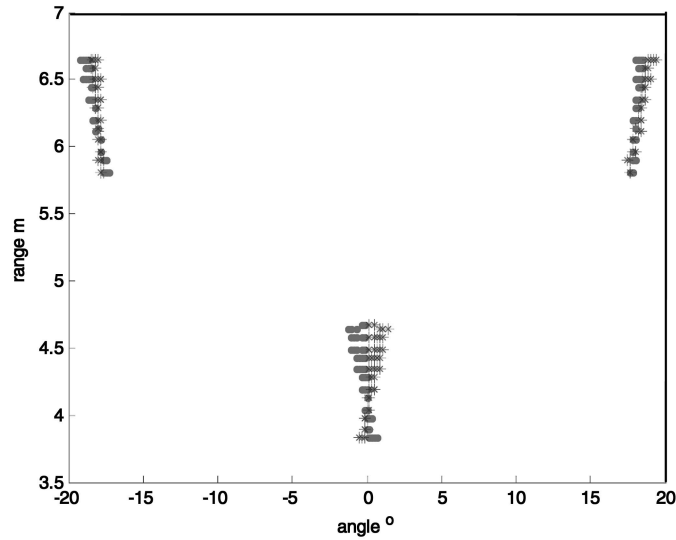
By using the pseudocode provided in Section IVC, we obtain  $\hat{d} = 0.50$  for  $\varepsilon_e = 6.25$  and  $\hat{d} = 0.3171$  for  $\varepsilon_e = 12.25$ . The polynomial orders  $r_1 = \tilde{r}_1 = r_2 = \tilde{r}_2 = 1$  in the pseudocode presented in Section IV are used to estimate the above two values of  $\hat{d}$ . The imaging results are shown in Fig. 15(a) and (b) with the two wall parameter pairs  $(\varepsilon_e, d_e) = (6.25, 0.50)$  and  $(\varepsilon_e, d_e) = (12.25, 0.3171)$ , respectively. It is clear that while these two pairs represent incorrect values of the wall parameters, they can be used to generate good images for all three targets.

## VI. CONCLUSIONS

The effects of unknown wall parameters on the TWI quality are two-fold; blurriness and shifting. This paper has proposed an approach in which the different shifts in the imaged target positions due to different assumed wall parameters are utilized to provide reliable imaging under wall parameter ambiguities. Imaging is performed using wideband pulses and coherent combining. For a given transmit and receive array antenna structure, the scene behind the wall is imaged assuming various values of the dielectric constant and wall thickness parameters. A trajectory of the shifts in each target position is generated. The above steps are repeated using a different array structure. In this paper, we move the transmit array antennas equally in one direction, and keep the receive array unchanged. The intersection of the two trajectories, corresponding to the two array structures, is taken as the estimate of the target position. The proposed approach was analyzed to examine the orientations of target trajectories in the



(a)



(b)

Fig. 14. Finding true position of targets with wall parameter errors. (a)  $\varepsilon_e = 12.25$ ,  $\pi = 9$ , wall error 0.25 0.20 0.15 0.1 0.05 0 -0.05 -0.1 -0.15 -0.20 -0.25 -0.3. (b)  $\varepsilon_e = 6.26$ ,  $\pi = 9$ , wall error 0.25 0.20 0.15 0.1 0.05 0 -0.05 -0.1 -0.15 -0.20 -0.25 -0.3.

range-angle domain. Fundamental to our approach was to show that these orientations depend on the target locations relative to the array center. Computer simulations using two and multiple array structures were represented and have demonstrated satisfactory target location estimations. The paper has considered a coherent imaging approach. The noncoherent approach for TWI is discussed in [21] and [22]. It is noted that the proposed technique has been introduced assuming point targets. Performance under spatially extended targets requires further analyses and simulations.

#### APPENDIX A

For simplicity, we only consider the traveling time from a transmit antenna to the target. The traveling

time from the target to a receiver antenna can be formulated similarly. As shown in Fig. 5, without errors in the wall thickness,

$$x_{p,m} = d \tan(\theta_{t_m,p}) + h \tan(\varphi_{t_m,p}) \quad (33)$$

where  $h = z_p - d$ . We consider the traveling time when there is an error  $\Delta d = d_e - d$  in the wall thickness. When  $d$  changes to  $d + \Delta d$  (and subsequently  $h$  changes to  $h - \Delta d$ ) and  $\varphi_{t_m,p}$  changes to  $\varphi_{t_m,p} + \Delta\varphi_{t_m,p}$  (and subsequently  $\theta_{t_m,p}$  changes to  $\theta_{t_m,p} + \Delta\theta_{t_m,p}$ ), the change in  $x_{p,m}$  can be approximated by

$$\begin{aligned} \Delta x_{p,m} &= \frac{\partial x_{p,m}}{\partial d} \Delta d + \frac{\partial x_{p,m}}{\partial h} \Delta h + \frac{\partial x_{p,m}}{\partial \theta_{t_m,p}} \Delta \theta_{t_m,p} + \frac{\partial x_{p,m}}{\partial \varphi_{t_m,p}} \Delta \varphi_{t_m,p} \\ &= \tan(\theta_{t_m,p}) \Delta d + \tan(\varphi_{t_m,p}) \Delta h + d \cos^{-2}(\theta_{t_m,p}) \Delta \theta_{t_m,p} \\ &\quad + h \cos^{-2}(\varphi_{t_m,p}) \Delta \varphi_{t_m,p}. \end{aligned} \quad (34)$$

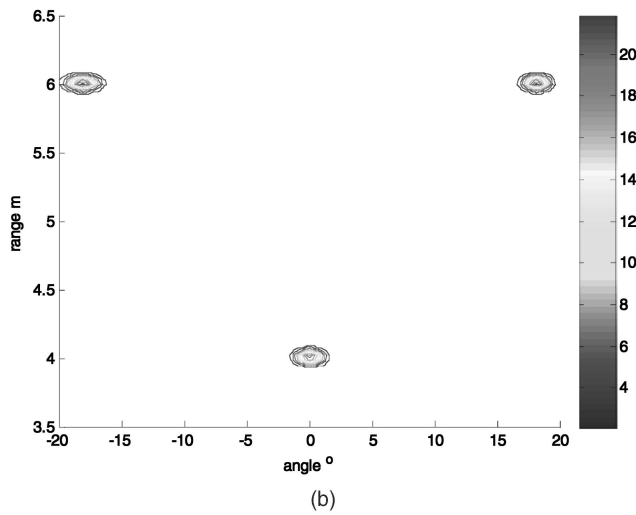
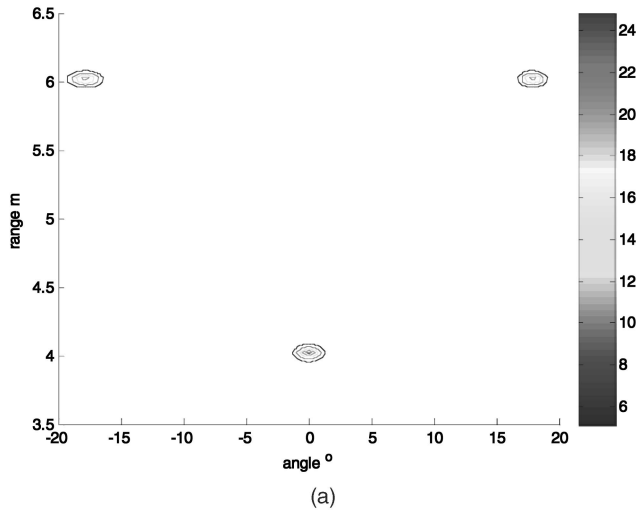


Fig. 15. Imaging with estimated wall parameter pair. (a) Image result with pair  $(\varepsilon_e, d_e) = (6.25, 0.50)$ . (b) Image result with pair  $(\varepsilon_e, d_e) = (12.25, 0.3171)$ .

For the path to pass through the true target position,  $\Delta x_{p,m} = 0$ . That is,

$$\begin{aligned} \Delta d \tan(\theta_{t_m,p}) + \Delta h \tan(\varphi_{t_m,p}) + d \cos^{-2}(\theta_{t_m,p}) \Delta \theta_{t_m,p} \\ + h \cos^{-2}(\varphi_{t_m,p}) \Delta \varphi_{t_m,p} = 0. \end{aligned} \quad (35)$$

From the Snell's law,

$$\sin(\varphi_{t_m,p}) = \sqrt{\varepsilon} \sin(\theta_{t_m,p}) \quad (36)$$

we have

$$\cos(\varphi_{t_m,p}) \Delta \varphi_{t_m,p} = \sqrt{\varepsilon} \cos(\theta_{t_m,p}) \Delta \theta_{t_m,p}$$

that is,

$$\Delta \theta_{t_m,p} = \Delta \varphi_{t_m,p} \frac{\cos(\varphi_{t_m,p})}{\sqrt{\varepsilon} \cos(\theta_{t_m,p})}. \quad (37)$$

Substituting (37) in (35) yields

$$\begin{aligned} \Delta d \tan(\theta_{t_m,p}) + \Delta h \tan(\varphi_{t_m,p}) + \frac{d}{\sqrt{\varepsilon}} \cos^{-3}(\theta_{t_m,p}) \cos(\varphi_{t_m,p}) \Delta \varphi_{t_m,p} \\ + h \cos^{-2}(\varphi_{t_m,p}) \Delta \varphi_{t_m,p} = 0. \end{aligned} \quad (38)$$

Since  $\Delta h = -\Delta d$ , then

$$\Delta \varphi_{t_m,p} = \frac{\Delta d [\tan(\varphi_{t_m,p}) - \tan(\theta_{t_m,p})]}{\frac{d \cos(\varphi_{t_m,p})}{\sqrt{\varepsilon} \cos^3(\theta_{t_m,p})} + \frac{h}{\cos^2(\varphi_{t_m,p})}}. \quad (39)$$

(39) shows the necessary shift of the incident angles for the path traveling from the  $m$ th antenna to the point  $p$  when the wall thickness error is taken into account. On the other hand, the total travel time from the  $m$ th antenna to the target position  $p$  is given by

$$\tau_{p,m} = \frac{1}{c} \left( \frac{\sqrt{\varepsilon} d}{\cos(\theta_{t_m,p})} + \frac{h}{\cos(\varphi_{t_m,p})} \right). \quad (40)$$

Therefore, the additional travel time due to  $\Delta d$  and  $\Delta \varphi_{t_m,p}$  can be expressed using first-order approximation as

$$\begin{aligned} \Delta \tau_{p,m} &= \frac{\partial \tau_{p,m}}{\partial d} \Delta d + \frac{\partial \tau_{p,m}}{\partial \theta_{t_m,p}} \Delta \theta_{t_m,p} + \frac{\partial \tau_{p,m}}{\partial \varphi_{t_m,p}} \Delta \varphi_{t_m,p} \\ &= \frac{\partial \tau_{p,m}}{\partial d} \Delta d + \Delta \varphi_{t_m,p} \left( \frac{\partial \tau_{p,m}}{\partial \theta_{t_m,p}} \frac{\cos(\varphi_{t_m,p})}{\sqrt{\varepsilon} \cos(\theta_{t_m,p})} + \frac{\partial \tau_{p,m}}{\partial \varphi_{t_m,p}} \right) \\ &= \frac{\Delta d}{c} \left( \frac{\sqrt{\varepsilon}}{\cos(\theta_{t_m,p})} - \frac{1}{\cos(\varphi_{t_m,p})} \right) + \frac{\Delta \varphi_{t_m,p}}{c} \\ &\quad \times \left( \frac{d \cos(\varphi_{t_m,p})}{\cos^2(\theta_{t_m,p})} \tan(\theta_{t_m,p}) + \frac{h}{\cos(\varphi_{t_m,p})} \tan(\varphi_{t_m,p}) \right) \\ &= \frac{\Delta d}{c} \left( \frac{\sqrt{\varepsilon}}{\cos(\theta_{t_m,p})} - \frac{1}{\cos(\varphi_{t_m,p})} \right) \\ &\quad + \frac{\Delta d}{c} \frac{[\tan(\varphi_{t_m,p}) - \tan(\theta_{t_m,p})]}{\frac{d \cos(\varphi_{t_m,p})}{\sqrt{\varepsilon} \cos^3(\theta_{t_m,p})} + \frac{h}{\cos^2(\varphi_{t_m,p})}} \\ &\quad \times \left( \frac{d \cos(\varphi_{t_m,p})}{\cos^2(\theta_{t_m,p})} \tan(\theta_{t_m,p}) + \frac{h}{\cos(\varphi_{t_m,p})} \tan(\varphi_{t_m,p}) \right) \\ &= \frac{\Delta d}{c} \left( \frac{\sqrt{\varepsilon}}{\cos(\theta_{t_m,p})} - \frac{1}{\cos(\varphi_{t_m,p})} \right) \\ &\quad + \frac{\Delta d}{c} [\tan(\varphi_{t_m,p}) - \tan(\theta_{t_m,p})] \sin(\varphi_{t_m,p}) \\ &= \frac{\Delta d}{c} [\sqrt{\varepsilon} \cos(\theta_{t_m,p}) - \cos(\varphi_{t_m,p})] \\ &= \frac{\Delta d \sin(\varphi_{t_m,p} - \theta_{t_m,p})}{c \sin(\theta_{t_m,p})}. \end{aligned} \quad (41)$$

## APPENDIX B

We consider the situation where there is an error in the estimated value of the dielectric constant of the wall material,  $\Delta \varepsilon = \varepsilon_e - \varepsilon$ . The incident angles are adjusted so that the new path links the  $m$ th antenna and the target point  $p$ . From (33), we obtain the

following first-order approximation,

$$\begin{aligned}\Delta x_{p,m} &= \frac{\partial x_{p,m}}{\partial \theta_{t_m,p}} \Delta \theta_{t_m,p} + \frac{\partial x_{p,m}}{\partial \varphi_{t_m,p}} \Delta \varphi_{t_m,p} \\ &= \frac{\Delta \theta_{t_m,p} d}{\cos^2(\theta_{t_m,p})} + \frac{\Delta \varphi_{t_m,p} d}{\cos^2(\varphi_{t_m,p})}.\end{aligned}\quad (42)$$

For the path to pass through the true target position,  $\Delta x_{p,m} = 0$ . That is,

$$\frac{\Delta \theta_{t_m,p} d}{\cos^2(\theta_{t_m,p})} + \frac{\Delta \varphi_{t_m,p} d}{\cos^2(\varphi_{t_m,p})} = 0.\quad (43)$$

From (41), the additional time due to the error  $\Delta \varepsilon$  becomes

$$\begin{aligned}\Delta \tau_{p,m} &= \frac{\partial \tau_{p,m}}{\partial \varepsilon} \Delta \varepsilon + \frac{\partial \tau_{p,m}}{\partial \theta_{t_m,p}} \Delta \theta_{t_m,p} + \frac{\partial \tau_{p,m}}{\partial \varphi_{t_m,p}} \Delta \varphi_{t_m,p} \\ &= \frac{1}{c} \left( \frac{\Delta \varepsilon}{2\sqrt{\varepsilon}} \frac{d}{\cos(\theta_{t_m,p})} + \frac{\sqrt{\varepsilon} d \sin(\theta_{t_m,p})}{\cos^2(\theta_{t_m,p})} \Delta \theta_{t_m,p} + \frac{h \sin(\varphi_{t_m,p})}{\cos^2(\varphi_{t_m,p})} \Delta \varphi_{t_m,p} \right) \\ &= \frac{1}{c} \left( \frac{\Delta \varepsilon}{2\sqrt{\varepsilon}} \frac{d}{\cos(\theta_{t_m,p})} + \sin(\varphi_{t_m,p}) \left( \frac{d \Delta \theta_{t_m,p}}{\cos^2(\theta_{t_m,p})} + \frac{h \Delta \varphi_{t_m,p}}{\cos^2(\varphi_{t_m,p})} \right) \right) \\ &= \frac{\Delta \varepsilon}{2c\sqrt{\varepsilon}} \frac{d}{\cos(\theta_{t_m,p})}.\end{aligned}\quad (44)$$

## REFERENCES

- [1] Ferris, D. D., Jr., and Currie, N. C. A survey of current technologies for through-the-wall surveillance (TWS). *Proceedings of SPIE*, **3577** (Nov. 1998), 62–72.
- [2] Nag, S., Fluhler, H., and Barnes, M. Preliminary interferometric images of moving targets obtained using a time-modulated ultra-wide band through-wall penetration radar. In *Proceedings of IEEE Radar Conference*, May 2001, 64–69.
- [3] Wild, N. C., Felber, F., Treadaway, M., Doft, F., Breuner, D., and Lutjens, S. Ultrasonic through-the wall surveillance system. *Proceedings of SPIE*, **4232** (2001), 167–176.
- [4] Falconer, D. G., Steadman, K. N., and Watters, D. G. Through-the wall differential radar. *Proceedings of SPIE*, **2938** (Nov. 1996), 147–151.
- [5] Greneker, E. F. RADAR flashlight for through-the-wall detection of humans. *Proceedings of SPIE*, **3375** (Apr. 1998), 280–285.
- [6] Black, J. D. Motion and ranging sensor through-the-wall surveillance system. *Proceedings of SPIE*, **4708** (2002), 114–121.
- [7] Hunt, A. R. Stepped-frequency CW radar for concealed weapon detection and through-the-wall surveillance. *Proceedings of SPIE*, **4708** (2002), 99–105.
- [8] Nag, S., et al. An ultra-wideband through-the-wall radar for detecting the motion of people in real time. *Proceedings of SPIE*, **4744** (2002), 48–57.
- [9] Falconer, D. G., Ficklin, R. W., and Konolige, K. G. Detection, location, and identification of building occupants using a robot-mounted through-wall radar. *Proceedings of SPIE*, **4037** (2000), 72–81.
- [10] Choi, W., and Sarkar, T. Echo cancellation using a homomorphic deconvolution. Presented at IEEE AP-S International Symposium and USNC/URSI National Radio Science Meeting, Monterey, CA, June 2004.
- [11] Hunt, A. R. Image formation through walls using a distributed radar sensor network. Presented at IEEE AP-S International Symposium and USNC/URSI National Radio Science Meeting, Monterey, CA, June 2004.
- [12] Frazier, L. M. Radar surveillance through solid materials. *Proceedings of SPIE*, **2938** (Nov. 1996), 139–146.
- [13] Ahmad, F., and Amin, M. G., Kassam, S. A., and Frazer, G. J. A wideband, synthetic aperture beamformer for through-the-wall imaging. In *Proceedings of the IEEE International Symposium on Phase Array Systems and Technology*, Boston, MA, Oct. 2003.
- [14] Ahmad, F., and Amin, M. G., and Kassam, S. A. Through-the-wall wideband synthetic aperture beamformer. *IEEE AP-S International Symposium 2004 Digest*, vol. 3, June 2004, Monterey, CA, 3059–3062.
- [15] Hoor, R. T., and Kassam, S. A. The unifying role of the coarray in aperture synthesis for coherent and incoherent imaging. *Proceedings of the IEEE*, **78**, 4 (Apr. 1990), 735–752.
- [16] Ahmad, F., Frazer, G. J., Kassam, S. A., and Amin, M. G. Design and implementation of near-field, wideband synthetic aperture beamforms. *IEEE Transactions on Aerospace and Electronic Systems*, **40**, 1 (2004), 206–220.
- [17] Ta-Hsin, L., and Ke-Shin, L. Deblurring two-tone images by a joint estimation approach using higher-order statistics. In *Proceedings of the IEEE Signal Processing Workshop on Higher-Order Statistics*, Banff, Canada, 1997.
- [18] Alparone, L., Argenti, F., Aiazzi, B., and Baronti, S. Multiresolution approaches to adaptive speckle reduction in synthetic aperture radar images. In *Proceedings of 2003 International Conference on Image Processing*, vol. 1, Barcelona, Spain, 2003.
- [19] Fortune, S., Hayes, M., and Gough, P. Statistical autofocus of synthetic aperture sonar images using image contrast optimization. *OCEANS 2001*, vol. 1, IEEE, Honolulu, HI, <http://www.darpa.mil/ato/programs/netex/models.pdf>.
- [20] Ahmad, F., and Amin, M. G. A noncoherent radar system approach for through-the wall imaging. *Proceedings of SPIE*, Mar. 28–Apr.1, 2005.
- [21] Ahmad, F., and Amin, M. G. A noncoherent system approach to through-the-wall radar imaging. In *Proceedings of IEEE Ap-S International Symposium*, 2005.
- [22] Ahmad, F., Tchangov, T., Kassam, S. A., and Amin, M. G. Image quality measures for wall parameter estimation. Presented at IEEE International Symposium on Signal Processing and Information Technology, Darmstadt, Germany, Dec. 2003.
- [23] Ahmad, F., and Kassam, S. A. Coarray analysis of the wide-band point spread function for active array imaging. *Signal Processing*, **81** (Jan. 2001), 99–115.



**Genyuan Wang** received the B.Sc. and M.S. degrees in mathematics from Shaanxi Normal University, Xi'an, China, in 1985 and 1988, respectively. He received his Ph.D. degree in electrical engineering from Xidian University, Xi'an China, in 1998.

From 1988 to 1994, he worked at Shaanxi Normal University as an assistant professor and then an associate professor. From 1994 to 1998, he worked at Xidian University as a research assistant. He worked with the Department of Electrical and Computer Engineering, University of Delaware as a post-doctoral fellow. Currently, he works with the Center of Advanced Communications, Villanova University, as a research associate. His research interests are radar imaging, radar signal processing, adaptive filter, OFDM system, channel equalization, channel coding, space-time coding, and multiple-input multiple-output for broadband wireless communication systems.



**Moeness Amin** (F'00) received his Ph.D. degree in electrical engineering in 1984 from the University of Colorado, Boulder.

He has been on the faculty of Villanova University since 1985, where is now a professor in the Department of Electrical and Computer Engineering and the Director of the Center for Advanced Communications.

Dr. Amin is the recipient of the IEEE Third Millennium Medal, Distinguished Lecturer of the IEEE Signal Processing Society for 2003–2004, member of the Franklin Institute Committee on Science and the Arts, and recipient of the 1997 Villanova University Outstanding Faculty Research Award, recipient of the 1997 IEEE Philadelphia Section Service Award. He has over 300 publications in the areas of wireless communications, time-frequency analysis, smart antennas, interference cancellation in broadband communication platforms, digitized battlefield, direction finding, over the horizon radar, radar imaging, and channel equalizations.



**Yimin Zhang** (SM'01) received his Ph.D. degree from the University of Tsukuba, Tsukuba, Japan, in 1988.

He joined the faculty of the Department of Radio Engineering, Southeast University, Nanjing, China, in 1988. He served as a technical manager at the Communication Laboratory Japan, Kawasaki, Japan, from 1995 to 1997, and was a visiting researcher at ATR Adaptive Communications Research Laboratories, Kyoto, Japan, from 1997 to 1998. Since 1998, he has been with the Villanova University, where he is currently a research associate professor at the Center for Advanced Communications and the Director of the Radio Frequency Identification (RFID) Lab. His research interests are in the areas of array signal processing, space-time adaptive processing, multiuser detection, MIMO systems and cooperative diversity, blind signal processing, digital mobile communications, and time-frequency analysis.